



# Investigations on the pyrolysis characteristics of sludge and peanut shell: thermal decomposition behaviors, kinetic, products

Ming Zhao<sup>1</sup> · Donghua Ji<sup>2</sup>

Received: 19 February 2024 / Revised: 9 April 2024 / Accepted: 15 April 2024  
© The Author(s), under exclusive licence to Springer-Verlag GmbH Germany, part of Springer Nature 2024

## Abstract

Paper mill sludge is an industrial waste that can cause environmental pollution if not handled properly. As a common agricultural waste, peanut shells are abundant in production. This study aimed to investigate the thermal decomposition behavior, kinetics, and distribution of pyrolysis products of both sludge and peanut shells. Thermogravimetric analysis revealed that the pyrolysis process of sludge and peanut shells can be divided into three stages: drying pre-pyrolysis, main pyrolysis, and carbonization. As the heating rate increases, the TG curve and DTG curve shift toward higher temperatures, leading to thermal hysteresis in the main pyrolysis region. This phenomenon shortens the pyrolysis time and increases the maximum weight loss rate. Additionally, the higher the peanut shell content, the lower the residual mass and the higher the weight loss rate. The Coats-Redfern method was employed to calculate the pyrolysis kinetics, and the fitting correlation coefficients were all greater than 0.98 when the reaction order  $n = 1$ , indicating a good fitting effect. The activation energies ranged from 31.85 to 35.12 kJ/mol at different heating rates and 27.90 to 31.85 kJ/mol at different peanut shell contents. Py-GC/MS analysis of the pyrolysis products of sludge revealed a predominance of hydrocarbons, acids and furans, with a relatively high content of acids. In contrast, the pyrolysis products of peanut shells mainly consisted of ketones in varying types and contents. These research findings provide a theoretical foundation for understanding the fuel characteristics and high-value utilization of sludge and peanut shells.

**Keywords** Sludge · Coconut shell · Pyrolysis · Kinetic · Py-GC/MS

## 1 Introduction

Paper mill sludge is the residue of papermaking, containing various organic matter, heavy metals, and other substances that pose risks to the environment and public health [1]. The China Paper Association reported that paper production in China

reached approximately 283.91 million tons in 2022, resulting in an average of 1 m<sup>3</sup> of sludge per ton of paper [2, 3]. The disposal of such large quantities of paper mill sludge presents a complex problem. Currently, common treatment methods include landfilling, agricultural utilization, and incineration [4]. However, these methods may lead to secondary pollution [5]. Similarly, peanut shells, as agricultural residues, are produced in massive quantities, and improper disposal will inevitably cause environmental pollution and resource wastage. Reports indicate that China accounts for approximately 40% of global peanut production, with an annual output of 16.68 million tons, resulting in a significant amount of peanut shell waste [6]. Given the adverse effects of paper mill sludge and peanut shell waste, it is imperative to develop environmentally friendly and resource-based approaches for their utilization.

Pyrolysis technology involves the thermal decomposition of raw materials under hypoxic conditions. It is a straightforward process that can convert waste into solids, liquids, and gases [7]. Sludge, due to its high organic matter content, can also be considered a potential biological resource. Through pyrolysis technology, the organic matter in sludge can be

### Highlights

- Sludge and peanut shell were used for resource utilization.
- The thermal decomposition behavior was investigated.
- The Coats-Redfern method is more reliable to calculate the pyrolysis kinetics.
- Sludge and peanut shells are studied as raw materials for the production of chemicals.

✉ Ming Zhao  
zhaoming@seu.edu.cn

<sup>1</sup> Key Laboratory of Energy Thermal Conversion and Control of Ministry of Education, School of Energy and Environment, Southeast University, Nanjing 210096, China

<sup>2</sup> Japhl Powertrain Systems CO., LTD, Nanjing 210000, China

converted into energy, resulting in the production of biochar, biooil, and biogas [8]. Biochar can be utilized in the production of carbon materials like activated carbon, while biooil can serve as aviation fuel. Biogas, on the other hand, can be used as a raw material in various industries or for heating and power generation purposes. Gao et al. [9] conducted a study on the slow pyrolysis of sludge. The oil produced at a temperature of 700 °C contained a significant amount of phenols and esters, while most of the heavy metals in the sludge were retained in the carbon, thereby achieving the high-value and environmentally friendly utilization of sludge. Another study by Wang et al. [10] involved the co-pyrolysis of rice husk and sludge, which demonstrated improved pyrolysis behavior. The addition of 30% rice husk resulted in the lowest activation energy and showed a synergistic effect of volatiles during co-pyrolysis. The addition of other materials, such as lignocellulosic and municipal waste, to the sludge increases the carbon source, thereby promoting the comprehensive utilization of the sludge. When comparing sludge pyrolysis with co-pyrolysis with MSW, it is observed that the apparent activation energy is significantly reduced in the latter case, suggesting that co-pyrolysis reduces the energy consumption of the reaction [11]. Hazelnut shell, as a new type of biomass, possesses low ash content and abundant hydrocarbon. Through co-pyrolysis with sludge, it can be effectively reused to mitigate pollution [12].

Currently, co-pyrolysis is still in the developmental stage and there have been limited studies on the co-pyrolysis characteristics and kinetics of sludge and peanut shells. This study aims to investigate the thermal decomposition behavior, kinetic characteristics, and product distribution of sludge and peanut shells using TG, Coats-Redfern method kinetic fitting, and Py-GC/MS techniques. Understanding the thermal decomposition behavior will provide insights into the fuel characteristics and thermal decomposition characteristics of sludge and peanut shells. Determining the pyrolysis kinetics parameters is crucial for designing efficient and economically feasible sludge and peanut shell treatment equipment. Additionally, evaluating the product distribution can help assess the potential of the sample for further chemical utilization. These findings are essential for advancing the clean and resourceful utilization of sludge and peanut shells in the future.

## 2 Materials and methods

### 2.1 Materials and equipment

This study utilized paper mill sludge obtained from Shandong Chenming Paper Co., LTD, and peanut shells sourced from Shangqiu City, Henan Province, China, as feedstocks. The raw materials were purified and then naturally dried in a cool and dark environment. The dried samples were finely ground using

a grinder and sieved to obtain particles of approximately 0.2 mm in size (80 mesh). Afterward, the samples were further dried at 105 °C for 24 h in an oven and stored in airtight bags to maintain their integrity until further analysis.

The ultimate analysis of samples was performed using the Vario ELIII element analyzer (Elementar, Germany). The CHNS element was analyzed and determined by dynamic combustion method in CHNS mode. The proximate analysis methods and procedures were referred to the Proximate Analysis of Solid Biofuels of China (GB/T 28731-2012). The higher heating value (HHV) was determined by an automatic calorimeter (XKRL-3000A, Henan Xinke Analytical Instrument, China). Biomass components (cellulose, hemicellulose, lignin) were tested according to NREL 2007 Determination of Structural Carbohydrates and Lignin in Biomass. The pyrolysis experiment of feedstocks was carried out with a synchronous thermal analyzer (STA409PC, NETZSCH, Germany). Samples weighing 6–7 mg were placed in an alumina crucible and subsequently analyzed using a synchronous thermal analyzer. The pyrolysis temperature was gradually increased from room temperature to 800 °C at various heating rates. The carrier gas and shielding gas were both high purity nitrogen (99.99%) with flow rates of 30 mL/min and 20 mL/min, respectively. In order to facilitate identification, the samples of X% (10%, 20%, and 30%) peanut shell mixed with (100 – X)% sludge were named as 10%Ps/90%S, 20%Ps/80%S, and 30%Ps/70%S, where Ps represents peanut shell and S represents sludge.

### 2.2 Kinetics reactions in pyrolysis

Biomass can be decomposed into fixed carbon and volatile gases through heat. The pyrolysis process of biomass can be described as A (solid) → B (solid) + C (gas). Nitrogen is used as a continuous purge gas during the test to prevent any secondary reactions. The kinetic equation is shown as follows:

Isothermal homogeneous process:

$$d\alpha/dt = kf(\alpha) \quad (1)$$

Non-isothermal heterogeneous processes:

$$d\alpha/dT = kf(\alpha)/\beta \quad (2)$$

$$\beta = dT/dt \quad (3)$$

$$\alpha = (m_o - m_t)/(m_o - m_f) \quad (4)$$

$$k = Ae^{-E/RT} \quad (5)$$

where  $\alpha$  is the conversion rate in the reaction process, %;  $m_o$  is the initial mass of the sample, g;  $m_f$  is the final weight of the sample after the reaction, g;  $m_t$  is the mass of sample at time  $t$ , g;  $k$  is the kinetic constant;  $f(\alpha)$  is the reaction

mechanism function;  $A$  refers to the pre-exponential factor,  $\text{min}^{-1}$ ;  $E$  is the activation energy,  $\text{kJ/mol}$ ;  $R$  is the molar gas constant,  $R = 8.314 \text{ J/(mol}\cdot\text{K)}$ ;  $T$  is the reaction temperature,  $\text{K}$ ;  $\beta$  is the heating rate,  $^{\circ}\text{C/min}$ ;  $t$  is the time,  $\text{min}$ .

The reaction mechanism function is

$$f(\alpha) = (1-\alpha)^n \quad (6)$$

By integrating Eqs. (2), (5) and (6), the kinetic equation can be obtained as follows:

$$d\alpha/dT = A(1-\alpha)^n \exp(-E/RT)/\beta \quad (7)$$

The reaction model, pre-exponential factor, and activation energy of the sample can be determined by kinetic analysis of the pyrolysis process. The Coats-Redfern method was used to calculate the pyrolysis kinetic parameters, and Eq. (7) was treated to obtain the following:

When  $n = 1$ ,

$$\ln \left[ -\frac{\ln(1-\alpha)}{T^2} \right] = \ln \left[ \frac{AR}{E\beta} \left( 1 - \frac{2RT}{E} \right) \right] - \frac{E}{RT} \quad (8)$$

When  $n \neq 1$ ,

$$\ln \left[ \frac{1 - (1-\alpha)^{1-n}}{T^2(1-n)} \right] = \ln \left[ \frac{AR}{E\beta} \left( 1 - \frac{2RT}{E} \right) \right] - \frac{E}{RT} \quad (9)$$

For the general reaction region,  $2RT/E$  is much less than 1. So  $\ln \left[ \frac{AR}{E\beta} \left( 1 - \frac{2RT}{E} \right) \right]$  can be approximated as the constant  $\ln \left[ \frac{AR}{E\beta} \right]$ . When  $n \neq 1$ ,  $\ln \left[ \frac{1 - (1-\alpha)^{1-n}}{T^2(1-n)} \right]$  fits  $\frac{1}{T}$ ; when  $n = 1$ ,  $\ln \left[ -\frac{\ln(1-\alpha)}{T^2} \right]$  fits  $\frac{1}{T}$ . The slope is  $-\frac{E}{R}$  and the intercept is  $\ln \left[ \frac{AR}{E\beta} \right]$ , so that the activation energy  $E$  and the pre-exponential factor  $A$  can be calculated.

To comprehensively evaluate the pyrolysis characteristics of the sample, the comprehensive pyrolysis index (CPI) was defined as [13]

$$CPI = \frac{(-R_p) \cdot (-R_v) \cdot M_f}{T_i \cdot T_p \cdot \Delta T_{1/2}} \quad (10)$$

where  $R_v$  is the average decomposition rate;  $R_p$  is the maximum decomposition rate;  $M_f$  is weight loss ( $M_f = m_o - m_p$ );  $T_p$  is the peak temperature of DTG;  $T_i$  is the initial devolatilization temperature; and  $\Delta T_{1/2}$  is the half-peak wide temperature range when  $R/R_p = 0.5$ .

### 2.3 Py-GC/MS experiments

The pyrolysis products of sludge and peanut shell were determined using Py-GC/MS (Agilent GC7890A-MSD5975C, Agilent, USA). A 0.2-mg sample was weighed and placed into a quartz tube of a thermal cracker (CDS5200 Platinum

Wire Pyrolysis Analyzer). Quartz wool was used to secure the ends of the quartz tubes. The filled quartz tube was then placed in the center of the rapidly heated platinum wire. The initial temperature of the probe was  $20^{\circ}\text{C}$ , and it was heated at a rate of  $20^{\circ}\text{C/ms}$  until reaching the specified temperature. The GC/MS operating conditions were as follows: the injection ratio was 100:1, the injection port temperature was maintained at  $250^{\circ}\text{C}$ , and the helium flow rate was set to  $1 \text{ mL/min}$ . The programmed temperature curve consisted of holding the temperature at  $40^{\circ}\text{C}$  for 2 min, increasing it to  $200^{\circ}\text{C}$  at a heating rate of  $5^{\circ}\text{C/min}$ , further increasing it to  $280^{\circ}\text{C}$  at a heating rate of  $10^{\circ}\text{C/min}$ , and holding it for 3 min. The total run time of the analysis was 45 min. The compounds were separated using a capillary column (VF-1701ms,  $30 \text{ m} \times 0.25 \text{ mm i.d.} \times 0.25 \text{ }\mu\text{m.d.f.}$ ). The carrier gas in the column was helium with a purity of 99.999%, and the flow rate was maintained at  $1 \text{ mL/min}$ . The pyrolysis products and their relative contents were obtained by peak area percentage, using the NIST08 mass spectrometry database.

## 3 Results and discussion

### 3.1 Properties of feedstocks

To evaluate the feedstock properties of sludge and peanut shells during pyrolysis, a range of tests were conducted. These tests included ultimate analysis, proximate analysis, higher heating value (HHV), and component analysis, as presented in Table 1.

As the main element in biomass, C element is also the main combustible component of fuel. The carbon content of the sludge is 25.03% according to the ultimate analysis in Table 1. In comparison, the carbon content of the peanut shell is higher, reaching 51.18%. Therefore, adding peanut shells as a carburizing agent to the sludge can effectively increase the carbon content ratio of the raw material. This improvement enhances the flammability of the sludge-based fuel and facilitates the preparation of other products, such as sludge-based activated carbon [15]. The N and S elements in both feedstocks have relatively low content. Raw materials with low nitrogen and sulfur content offer advantages in the combustion or pyrolysis process. They generate fewer pollutants, such as  $\text{NO}_x$  and  $\text{SO}_x$ , during combustion, and produce fewer nitrogen and sulfur-containing gases during heat conversion. This reduction in polluting gas emission is beneficial.

After the water has been removed, the proximate analysis reveals that the sludge contains a lower amount of fixed carbon and consists mainly of volatile and ash components. The volatile content of the sludge, which is comparable to

**Table 1** Physicochemical analysis of sludge and peanut shell

Samples	Sludge	Peanut shell
Ultimate analysis (wt.%)		
C	25.03	51.18
H	4.33	7.39
N	2.78	1.91
S	0.93	0.10
O	33.44	37.02
Proximate analysis (wt.%)		
V	58.17	72.90
A	33.49	2.40
FC	8.34	24.70
HHV (MJ/kg)	11.56	17.44
Main composition		
Cellulose	17.87	31.79
Hemicellulose	14.91	19.82
Lignin	34.24	42.77
Others	32.98	5.62

FC = 100% - M - A - V [14], M = 0 on dry basis; O = 100% - M - A - C - H - N - S [13].

its organic content, is found to be 58.17%, indicating a relatively high organic content. Moreover, the high-temperature pyrolysis of the volatile content generates gases such as CO, CO<sub>2</sub>, H<sub>2</sub>, and CH<sub>4</sub>, where H<sub>2</sub> and CH<sub>4</sub> can be utilized for the production of clean energy [16]. On the other hand, the ash content represents the inorganic content, and the presence of alkali metals and other minerals in the ash can facilitate the pyrolysis process of biomass to some extent [17]. Additionally, peanut shells not only possess a high volatile content but also contain 24.7% fixed carbon. The primary component of fixed carbon is carbon, with small amounts of

hydrogen, oxygen, nitrogen, and other elements. The release of heat during biomass pyrolysis primarily stems from the fixed carbon. Consequently, a higher fixed carbon content results in a greater release of heat during pyrolysis.

The higher heating value (HHV) is an important measure of fuel, indicating the energy released when the feedstock is completely burned. Table 1 shows that the HHV of sludge is 11.56 MJ/kg, similar to that of peat (10.87–12.57 MJ/kg). On the other hand, peanut shell has an HHV of 17.44 MJ/kg, which is lower than that of bituminous coal (27.17–37.2 MJ/kg). The component analysis reveals that both sludge and peanut shell have significant amounts of lignin and cellulose. The lignin content of sludge is 34.24%, while peanut shell has a lignin content of 42.77%. These high lignin contents indicate that both feedstocks have high hardness and mechanical strength [18].

## 3.2 TGA and kinetic analysis

### 3.2.1 TGA of feedstocks individual

The TG and DTG curves of sludge and peanut shell at a heating rate of 10 °C/min are shown in Fig. 1. The pyrolysis performance of sludge and peanut shell at different stages is presented in Table 2. The pyrolysis process of sludge and peanut shells can be divided into three stages: drying pre-pyrolysis, main pyrolysis, and carbonization. The first stage primarily involves water precipitation and pre-pyrolysis. During this stage, the weight loss rate of sludge (temperature range: 25–226 °C) is 10.48%. The DTG curve exhibits a peak at 196.9 °C, indicating the highest weight loss rate of 0.75%/min during this stage. Similarly, the weight loss rate of peanut shell (temperature range: 25–210 °C) is 5.06%, with a peak at 64.8 °C and a corresponding weight loss rate

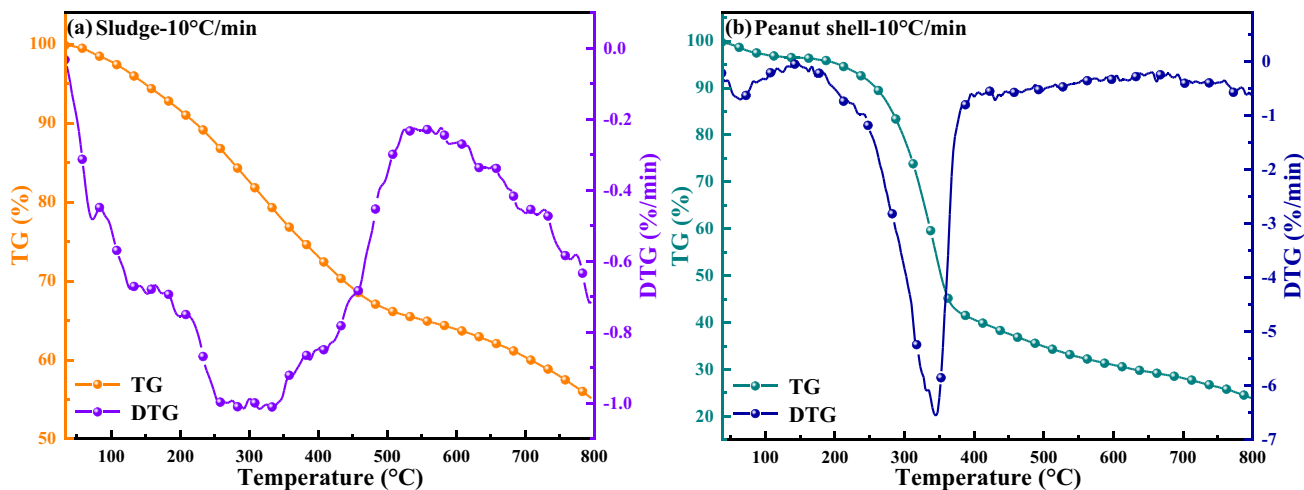


**Fig. 1** TG and DTG curves of feedstocks pyrolysis at 10 °C/min: **a** sludge; **b** peanut shell

**Table 2** Pyrolysis performance of sludge and peanut shell at various stages

Samples	Pyrolysis stage	Temperature range (°C)	Weight loss ratio (%)	Temperature of maximum weightlessness (°C)	Maximum weight loss (%/min)
Sludge	Drying pre-pyrolysis	25–226	10.48	196.9	0.75
	Main pyrolysis	226–446	20.27	314.7	1.02
	Carbonization	446–800	14.03	—	—
Peanut shell	Drying pre-pyrolysis	25–210	5.06	64.8	0.71
	Main pyrolysis	210–371	52.61	344	6.54
	Carbonization	371–800	18.24	—	—

of 0.71%/min. This heating process leads to the loss of free water, physical adsorption water, crystal water, and light volatile compounds in the samples [19].

The second stage of pyrolysis is the main stage. During this stage, the sludge (temperature range: 226–446 °C)

experiences a weight loss rate of 20.27%. The decomposition primarily involves large molecules such as cellulose and hemicellulose, which are transformed into small molecular gases and large molecular condensable volatile components. At a pyrolysis temperature of 314.7°C, there is a noticeable

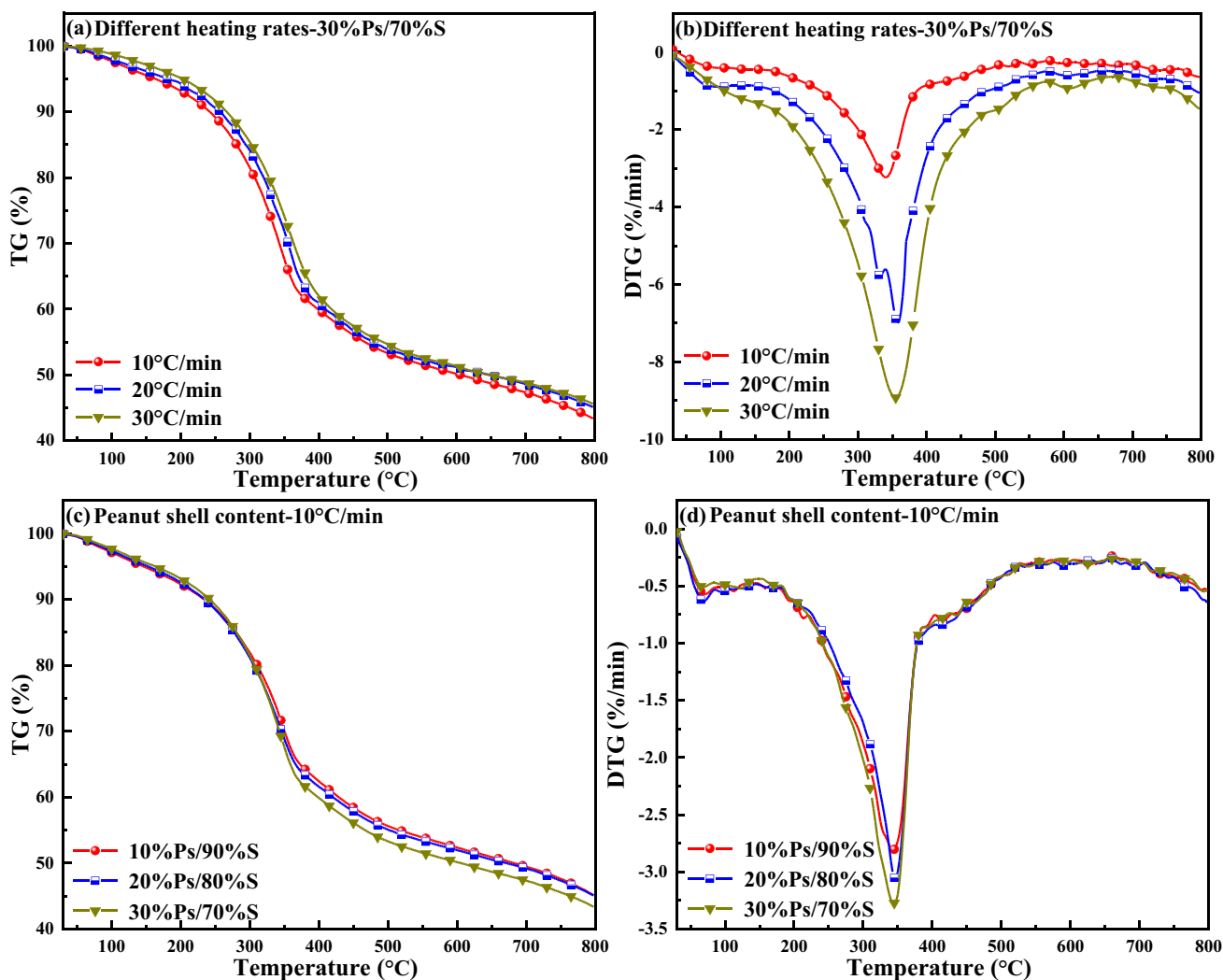


**Fig. 2** TG and DTG curves of feedstocks pyrolysis: **a, b** 30%Ps/70%S under different heating rates; **c, d** different peanut shell contents in sludge at 10 °C/min

**Table 3** Characteristic parameters of sample pyrolysis at various stages

Samples	Heating rate (°C/min)	Residual mass (%)	Total weight loss (%)	Point of maximum weightlessness		Main pyrolysis stage	
				Temperature (°C)	Weight loss (%/min)	Temperature range (°C)	Weight loss ratio (%)
10%Ps/90%S	10	45.12	54.80	342.5	2.81	292–389	19.83
20%Ps/80%S	10	44.10	55.82	347.5	3.05	282–388	21.63
30%Ps/70%S	10	43.37	56.58	348.8	3.31	282–386	25.53
30%Ps/70%S	20	45.12	54.25	354	7.00	295–393	23.41
30%Ps/70%S	30	45.59	54.37	355	8.93	298–405	21.49

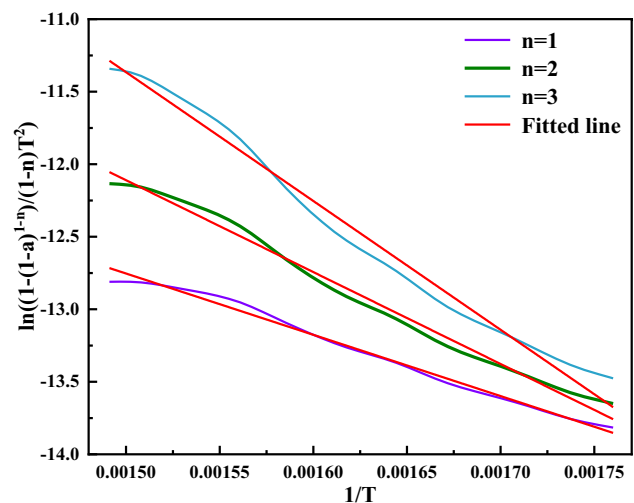
peak in sludge weight loss, resulting from the release of volatiles during the pyrolysis of cellulose, lignin, and protein [20]. Similarly, the peanut shell exhibits a weight loss rate of 52.61% in the temperature range of 210–371 °C, with two weight loss peaks observed in the DTG curve. The first peak, appearing around 331 °C, is not very prominent and is caused by the release of volatiles from the cellulose and lignin of the peanut shell. However, when the pyrolysis temperature reaches 344 °C, a sharp weight loss peak emerges, which is formed by the release of volatiles from the pyrolysis of cellulose and lignin. Hemicellulose, which mainly consists of easily hydrolyzed sugars, decomposes between 270 and 320 °C [21]. Previous studies by Lin et al. [22] indicated that cellulosic materials in sludge decomposed within the temperature range of 240–400 °C, while Han et al. [23] found that lignin decomposed at 200 °C, with a DTG peak observed at 340 °C. It is evident that the thermal decomposition of hemicellulose, cellulose, and lignin overlaps with each other during the main pyrolysis stage.

During the third stage, known as the carbonization stage, the pyrolysis of cellulose and hemicellulose in sludge (446–800 °C) and peanut shell (371–800 °C) is mostly completed. This stage primarily involves the pyrolysis of lignin and residues, resulting in further condensation of macromolecular organic matter. As a result, the weight loss rate is not obvious and the DTG curve tends to flatten during this stage.

### 3.2.2 TGA of feedstocks blend

Figure 2(a) and (b) displays the TG and DTG diagrams of the mixed samples (30%Ps/70%S) at different heating rates (10, 20, and 30 °C/min). Table 3 presents the corresponding pyrolysis characteristic parameters. The pyrolysis process of the sample can be divided into three stages: drying pre-pyrolysis, main pyrolysis, and carbonization. In the first stage, the temperature increases from 25 °C to approximately 130 °C, leading to the removal of water from the sample's surface. During this stage, the TG curve shows a slight decrease and the weight loss is weak. Subsequently, in the pre-pyrolysis stage, the sample undergoes

dehydration and drying, resulting in insignificant changes in the TG curve. It is generally believed that the removal of bound water from the raw material and a small amount of depolymerization occur during this stage. The second stage represents the main pyrolysis stage of the sample, characterized by complex chemical reactions that generate small molecular gases such as CO, CO<sub>2</sub>, and CH<sub>4</sub>, along with some volatile macromolecular substances that can coagulate. As a result, a significant amount of volatiles is precipitated [24]. With an increase in heating rate, the pyrolysis TG curve of the sample shifts toward the high temperature region. The time required for pyrolysis gradually decreases, while the residual mass gradually increases, indicating a reduction in the degree of pyrolysis reaction [4, 25]. It is generally believed that the main pyrolysis temperature is delayed by approximately 10 °C due to the influence of heating rate on heat and mass transfer between the inside and outside of the biomass, resulting in thermal hysteresis of pyrolysis [26, 27]. As the heating rate increases, the DTG curve of the sample also shifts toward the high temperature region, with corresponding temperatures of

**Fig. 3** Kinetic fitting line under different reaction order ( $n = 1, 2, 3$ )

**Table 4** Fitting results of pyrolysis kinetics of sample

Sample	Heating rate (°C/min)	<i>n</i>	Temperature range (°C)	Fitting equation	Correlation coefficient $R^2$
30%Ps/70%S	10	1	282–386	$y = -6.93 - 3830.40x$	0.98778
		2		$y = -3.47 - 5700.60x$	0.98716
		3		$y = -0.65 - 7946.60x$	0.98419

**Table 5** Kinetic fitting results of sample mechanism function

Samples	Heating rate (°C/min)	<i>n</i>	Temperature range (°C)	Fitting equation	$R^2$	<i>E</i> (kJ/mol)	<i>A</i> (min <sup>-1</sup> )
10%Ps/90%S	10	1	292–389	$y = -7.62 - 3437.64x$	0.98349	28.58	16.86
20%Ps/80%S	10	1	282–388	$y = -7.70 - 3355.73x$	0.98705	27.90	15.20
30%Ps/70%S	10	1	282–386	$y = -6.93 - 3830.40x$	0.98778	31.85	37.47
30%Ps/70%S	20	1	295–393	$y = -6.41 - 4224.55x$	0.99068	35.12	138.98
30%Ps/70%S	30	1	298–405	$y = -6.54 - 4030.77x$	0.98196	33.51	174.66

348.8 °C, 354 °C, and 355 °C, respectively. Moreover, the maximum weight loss rate gradually increases, indicating a more intense pyrolysis process. The third stage involves the carbonization of the sample, during which the TG curve changes slowly. The pyrolysis of hemicellulose and cellulose is mostly completed, while the pyrolysis of lignin and residues occurs at a slower pace.

Figure 2(c) and (d) displays the TG and DTG images of mixed samples containing varying amounts of peanut shell at a heating rate of 10 °C/min. Table 3 presents the pyrolysis parameters at different stages. The residual mass of the mixed samples gradually decreased as the peanut shell content increased. This can be attributed to the higher ash content in the sludge, resulting in greater retention. During the volatilization stage, the DTG curves for different peanut shell contents begin to diverge, with higher peanut shell content exhibiting a larger maximum weight loss rate. This is because the volatile content of peanut shell is higher compared to that of sludge. In the carbonization stage, there

is no significant differentiation among the samples, and the DTG curve tends to flatten [28].

### 3.2.3 Kinetic analysis of pyrolysis

The second stage is the main pyrolysis stage for various samples. To achieve a more accurate fitting, linear fitting is performed in the kinetic analysis of the second stage. Based on the derived kinetic equation, samples with a heating rate of 10 °C/min and a composition of 30%Ps/70%S were selected. Different reaction orders ( $n = 1, 2, 3$ ) were chosen for calculation. The results, as shown in Fig. 3 and Table 4, indicate that the correlation coefficient slightly decreases with an increase in reaction order. Therefore, the best kinetic fitting is obtained when  $n = 1$ .

The correlation coefficients of samples in different reaction orders ( $n = 1, 2, 3$ ) were compared. It was found that the best fitting effect was observed when  $n = 1$ . The kinetic fitting results of the sample are shown in Table 5 for  $n = 1$ . The

**Table 6** Comprehensive pyrolysis index (CPI) of samples

Samples	Heating rate (°C/min)	$R_p$ (%/min)	$R_v$ (%/min)	$M_f$ (%)	$T_p$ (°C)	$T_i$ (°C)	$\Delta T_{1/2}$ (°C)	CPI (10 <sup>-6</sup> % <sup>3</sup> °C <sup>-3</sup> min <sup>-2</sup> )
Sludge	10	1.02	0.59	44.78	314.7	224	381	1.00
Peanut shell	10	6.54	0.99	75.91	344.0	284	73	68.91
10%Ps/90%S	10	2.81	0.72	54.80	342.5	291	99	11.24
20%Ps/80%S	10	3.05	0.72	55.82	347.5	279	84	15.05
30%Ps/70%S	10	3.31	0.72	56.58	348.8	282	84	16.32
30%Ps/70%S	20	7.00	1.55	54.25	354.0	295	93	60.61
30%Ps/70%S	30	8.93	2.25	54.37	355.0	298	119	86.78

**Table 7** Types and contents of sludge pyrolysis products

Names	Olefins	Alkanes	Acids	Aromatics	Furans	Lipids	Nitriles	CO <sub>2</sub>	Others
Number of species	9	3	3	3	2	1	1	1	/
Relative content (%)	9.2	6.75	12.69	5.08	12.53	1.17	1.84	45.89	4.85

**Table 8** Types and contents of peanut shell pyrolysis products

Names	Ketones	Phenols	Aldehydes	Alcohols	Lipids	Acids	Sugars	CO <sub>2</sub>	Others
Number of species	8	7	7	2	2	1	1	1	/
Relative content (%)	23.81	11.78	16.5	7.26	3.22	9.12	4.25	17.42	6.64

results indicate that when  $n = 1$  is selected, the linear fitting correlation coefficients ( $R^2$ ) are all greater than 0.98, indicating a high linear fitting. The activation energies for different heating rates ranged from 31.85 to 35.12 kJ/mol, while those for different peanut shell contents ranged from 27.90 to 31.85 kJ/mol. With an increase in heating rate and peanut shell content, the activation energy ( $E$ ) showed an overall increasing trend. This increase was mainly attributed to the delayed heat transfer of the sample during pyrolysis. The pre-exponential factor ( $A$ ) also exhibited an upward trend, and there was a

certain kinetic relationship between the pre-exponential factor and the activation energy. Zaker et al. [29] conducted co-pyrolysis of low-density polyethylene with sludge and found that the activation energy of co-pyrolysis increased as the mixing ratio of low-density polyethylene increased. Liu et al. [30] demonstrated that the addition of corn stalks to sludge had a significant synergistic effect, resulting in a decrease in carbon yield, an increase in bio-oil yield, an increase in CO and CH<sub>4</sub> production, a decrease in activation energy, and a favorable pyrolysis reaction.

**Table 9** Pyrolysis products of sludge

No.	Compound name	Time (min)	Formula	Relative molecular mass	GC content (%)
1	Carbon dioxide	1.583	CO <sub>2</sub>	43.99	45.890
2	2,5-Diaminobenzene sulfonic acid	1.665	C <sub>6</sub> H <sub>8</sub> N <sub>2</sub> O <sub>3</sub> S	188.026	6.100
3	Cyclopropyl carbinol	1.731	C <sub>4</sub> H <sub>8</sub> O	72.058	2.679
4	1,3-Cyclopentadiene	2.025	C <sub>5</sub> H <sub>6</sub>	66.047	1.377
5	1-Hexene	2.145	C <sub>6</sub> H <sub>12</sub>	84.094	1.557
6	Acetonitrile	2.309	C <sub>2</sub> H <sub>3</sub> N	41.027	1.840
7	1-Heptene	2.98	C <sub>7</sub> H <sub>14</sub>	98.11	1.273
8	Benzene	3.149	C <sub>6</sub> H <sub>6</sub>	78.047	2.132
9	1-Octene	4.655	C <sub>8</sub> H <sub>16</sub>	112.125	0.823
10	Toluene	5.048	C <sub>7</sub> H <sub>8</sub>	92.063	2.457
11	1-Nonene	7.202	C <sub>9</sub> H <sub>18</sub>	126.141	1.022
12	Ethylbenzene	7.481	C <sub>8</sub> H <sub>10</sub>	106.078	0.494
13	phenylethylene	8.877	C <sub>8</sub> H <sub>8</sub>	104.063	0.921
14	1-Decene	10.208	C <sub>10</sub> H <sub>20</sub>	140.157	0.945
15	1-Undecene	13.285	C <sub>11</sub> H <sub>22</sub>	154.172	0.643
16	1-Dodecene	16.275	C <sub>12</sub> H <sub>24</sub>	168.188	0.622
17	1,6-anhydro-beta-D-manno-pyranose	32.88	C <sub>6</sub> H <sub>10</sub> O <sub>5</sub>	162.053	10.634
18	1,6-Anhydro-.beta.-D-glucofuranose	35.941	C <sub>6</sub> H <sub>10</sub> O <sub>5</sub>	162.053	1.909
19	Hexadecanoic acid	37.108	C <sub>16</sub> H <sub>32</sub> O <sub>2</sub>	256.24	3.823
20	1,2-Benzenedicarboxylic acid, dibutyl ester	37.185	C <sub>16</sub> H <sub>22</sub> O <sub>4</sub>	278.152	1.470
21	Octadecanoic acid	39.383	C <sub>18</sub> H <sub>36</sub> O <sub>2</sub>	284.272	2.781
22	Eicosane	41.718	C <sub>20</sub> H <sub>42</sub>	282.329	1.803
23	Docosane	42.542	C <sub>22</sub> H <sub>46</sub>	310.36	2.247



The comprehensive pyrolysis index (*CPI*) of the sample is presented in Table 6. Increasing the heating rate resulted in higher average ( $R_v$ ) and maximum decomposition rate ( $R_p$ ) of the sample, indicating a more intense release of volatile compounds during the pyrolysis process. The different peanut shell contents did not have a noticeable effect on this phenomenon. Conversely, decreasing the heating rate led to a gradual decrease in the initial devolatilization temperature ( $T_i$ ), making volatiles more prone to precipitation and resulting in a more complete pyrolysis process with a higher release of volatiles, which is beneficial for pyrolysis. The comprehensive pyrolysis index (*CPI*) increased significantly with the rise in heating rate, indicating that a higher heating rate enhances the reactivity of the sample and intensifies the pyrolysis reaction. However, the *CPI* value remained unaffected by the variation in peanut shell content [13]. Overall, the impact of heating rate on sample pyrolysis is more pronounced.

### 3.3 Product distribution by Py-GC/MS analysis

The sludge and peanut shell samples underwent rapid pyrolysis using Py-GC/MS. The composition of the pyrolysis products was determined using the peak area normalization method, and their chemical composition and relative content were identified using the NIST08 spectrum library. The types and contents of the pyrolysis products from the sludge and peanut shell samples are presented in Tables 7 and 8.

Based on the different chemical properties, sludge pyrolysis products can be classified into nine categories. Table 7 reveals that the main pyrolysis products of sludge primarily consist of olefins and alkanes, totaling 12 types. Among these, there are nine types of olefin compounds, such as 1,3-cyclopentadiene and 1-hexene, followed by three types of alkane compounds. Additionally, three types of acid compounds were detected, accounting for 12.69% of the volatile

**Table 10** Pyrolysis products of peanut shell

No.	Compound name	Time (min)	Formula	Relative molecular mass	GC content (%)
1	Carbon dioxide	1.594	CO <sub>2</sub>	43.99	17.424
2	Acetaldehyde	1.78	C <sub>2</sub> H <sub>4</sub> O	44.026	2.757
3	Methylglyoxal	2.156	C <sub>3</sub> H <sub>4</sub> O <sub>2</sub>	72.021	2.610
4	2,3-Butanedione	2.849	C <sub>4</sub> H <sub>6</sub> O <sub>2</sub>	86.037	1.265
5	3-Pentanone	3.067	C <sub>5</sub> H <sub>10</sub> O	86.073	1.021
6	Acetaldehyde, hydroxy	3.438	C <sub>2</sub> H <sub>4</sub> O <sub>2</sub>	60.021	4.822
7	Acetic acid glacial	4.131	C <sub>2</sub> H <sub>4</sub> O <sub>2</sub>	60.021	9.123
8	Hydroxyacetone	4.873	C <sub>3</sub> H <sub>6</sub> O <sub>2</sub>	74.037	4.372
9	Methyl acetate	7.595	C <sub>3</sub> H <sub>6</sub> O <sub>2</sub>	74.037	2.155
10	Butanedial	8.822	C <sub>4</sub> H <sub>6</sub> O <sub>2</sub>	86.037	2.433
11	Methyl pyruvate	8.866	C <sub>4</sub> H <sub>6</sub> O <sub>3</sub>	102.032	1.077
12	Furfural	9.264	C <sub>5</sub> H <sub>4</sub> O <sub>2</sub>	96.021	1.451
13	2-Hydroxy-2-cyclopenten-1-one	12.625	C <sub>5</sub> H <sub>6</sub> O <sub>2</sub>	98.037	1.898
14	2,4-Imidazolidinedione, 3-methyl-	14.916	C <sub>4</sub> H <sub>6</sub> N <sub>2</sub> O <sub>2</sub>	114.043	1.187
15	Methyl cyclopentenolone	15.527	C <sub>6</sub> H <sub>8</sub> O <sub>2</sub>	112.052	5.433
16	Phenol	16.765	C <sub>6</sub> H <sub>6</sub> O	94.042	3.216
17	Guaiacol	17.011	C <sub>7</sub> H <sub>8</sub> O <sub>2</sub>	124.052	1.513
18	2-Methoxy-4-methylphenol	19.93	C <sub>8</sub> H <sub>10</sub> O <sub>2</sub>	138.068	1.609
19	Cyclobutanol	20.022	C <sub>4</sub> H <sub>8</sub> O	132.042	6.365
20	Benzeneethanol,2-methoxy-	22.172	C <sub>9</sub> H <sub>12</sub> O <sub>2</sub>	152.084	0.888
21	Eugenol	24.31	C <sub>10</sub> H <sub>12</sub> O <sub>2</sub>	164.084	0.888
22	5-Hydroxymethyldihydrofuran-2-one	25.057	C <sub>5</sub> H <sub>8</sub> O <sub>3</sub>	116.047	4.026
23	Phenol,2-methoxy-4-(1Z)-1-propen-1-yl-	25.723	C <sub>10</sub> H <sub>12</sub> O <sub>2</sub>	164.084	1.165
24	(e)-isoeugenol	27.07	C <sub>10</sub> H <sub>12</sub> O <sub>2</sub>	164.084	1.181
25	Vanillin	27.501	C <sub>8</sub> H <sub>8</sub> O <sub>3</sub>	152.047	0.888
26	Acetovanillone	29.411	C <sub>9</sub> H <sub>10</sub> O <sub>3</sub>	166.063	4.635
27	D-Allose	32.94	C <sub>6</sub> H <sub>12</sub> O <sub>6</sub>	180.063	4.252
28	4-((1E)-3-Hydroxy-1-propenyl)-2-methoxyphenol	34.042	C <sub>10</sub> H <sub>12</sub> O <sub>3</sub>	180.079	2.212
29	4-Hydroxy-2-methoxycinnamaldehyde	35.93	C <sub>10</sub> H <sub>10</sub> O <sub>3</sub>	178.063	1.563

substances. Furthermore, two types of furan compounds constituted 12.53% of the detected volatile substances.

As shown in Table 8, peanut shells produce various pyrolysis products. Among these, ketones are the most diverse with a total of eight types. The main ketones identified are hydroxyacetone and methyl cyclopentenolone, constituting 23.81% of the volatile substances detected. Phenolic compounds, on the other hand, consist of seven types, with phenol and 2-methoxy-4-methylphenol being the predominant ones. These phenolic compounds account for 11.78% of the detected volatile substances. Additionally, there are seven types of aldehyde compounds, primarily acetaldehyde, hydroxy, and butanedial.

Table 9 shows that the sludge pyrolysis products primarily consist of hydrocarbon compounds, particularly olefins, which are mainly present from 2 to 16 min. The main olefins identified are 1,3-cyclopentadiene, 1-hexene, and 1-heptene. 1,3-cyclopentadiene can be utilized as an intermediate compound in organic synthesis. As a new catalyst, 1-hexene has high activity. 1-Heptene can be employed as an organic synthesis material for carbonyl synthesis of isooctanol. Alkane compounds containing cyclopropyl carbinol can serve as raw materials for the production of highly efficient flame retardants. Aromatic compounds accounted for 5.08% of the detected substances, primarily benzene, toluene, and ethylbenzene. Benzene finds applications in the production of synthetic detergents, dyes, organic pigments, fragrances, and pesticides. Ethylbenzene is mainly used as an intermediate in the petrochemical industry for the production of styrene [31]. Acid compounds constituted 12.69% of the total detected substances, with the main compounds being 2,5-diaminobenzene sulfonic acid, hexadecanoic acid, and octadecanoic acid. 2,5-Diaminobenzene sulfonic acid can be utilized as an intermediate compound in hair dye. Hexadecanoic acid is a saturated high fatty acid that can be used as a raw material for preparing composite phase change materials [32]. Octadecanoic acid can be employed as an additive in the industry to enhance the thermal stability of polyvinyl chloride (PVC) [33].

Table 10 reveals that peanut shells' pyrolytic products contain a higher concentration of ketones. Upon analyzing the detected peak area of each ketone product, it becomes evident that hydroxyacetone is the predominant ketone. Hydroxyacetone is a versatile additive with significant economic benefits, particularly in the cosmetics industry. Aldehyde compounds were primarily observed between 1 and 10 min, with acetaldehyde, hydroxy, and vanillin being the main products. Acetaldehyde, hydroxy is a crucial intermediate in organic synthesis and finds extensive applications in various industries such as chemical, food, medicine, and health. Vanillin, a fragrance widely utilized in cosmetics, household chemicals, and the food and beverage sectors,

was also detected [34]. Lipid compounds were concentrated in the 7-10 minutes range, primarily consisting of methyl acetate and methyl pyruvate. Methyl acetate serves as an organic solvent and finds widespread usage in the production of lacquered artificial leather and spices. Methyl pyruvate, a high-value fine chemical intermediate, is extensively employed in the pharmaceutical and pesticide fields [35]. Alcohol compounds, mainly cyclobutanol, were concentrated between 20 and 23 min. Cyclobutanol plays a vital role in the chemical synthesis of nitrogen-containing compounds and serves as a crucial synthetic intermediate.

## 4 Conclusions

This study investigated the pyrolysis characteristics of sludge and peanut shells through TG, Coats-Redfern method fitting, and Py-GC/MS experiments. The study calculated the pyrolysis parameters and kinetic parameters, and analyzed the pyrolysis products. Based on these findings, the following conclusions can be drawn.

- The pyrolysis process of sludge and peanut shell can be divided into three stages: drying pre-pyrolysis, main pyrolysis, and carbonization. As the heating rate increases, the TG curve shifts to the high temperature region, and thermal hysteresis occurs in the main pyrolysis region, which shortens the pyrolysis time and decreases the degree of pyrolysis reaction. The DTG curve also moves to the high-temperature region with an increase in the heating rate, causing an increase in the maximum weight loss rate. Additionally, a higher peanut shell content leads to a lower residual mass and a higher weight loss rate.
- When the Coats-Redfern method was employed to calculate the pyrolysis kinetic parameters, a reaction order of  $n = 1$  was utilized for kinetic analysis. The fitting correlation coefficients were all found to be greater than 0.98, indicating a satisfactory fitting effect. Moreover, as the heating rate and peanut shell content increased, both the activation energy ( $E$ ) and pre-exponential factor ( $A$ ) exhibited an upward trend.
- Based on their chemical properties, sludge pyrolysis products can be categorized into nine main groups, including olefins, alkanes, and acids, etc. Acid compounds, such as hexadecanoic acid and octadecanoic acid, and other fatty acids and their derivatives, are present in relatively high quantities. Pyrolysis products from peanut shells are also rich in variety, with ketones being one of the prominent types and present in significant amounts.

**Author contributions** Ming Zhao: conceptualization, methodology, experimental investigation, and writing—review and editing resources. Donghua Ji: validation, experimental investigation, and writing.

**Funding** This work was financially supported by the National Key Research and Development Program of China (2016YFD0600703-1).

**Data availability** Data will be available on request.

## Declarations

**Ethical approval** Not applicable.

**Consent to participate** Not applicable.

**Consent for publication** Not applicable.

**Competing interests** The authors declare no competing interests.

## References

- Bjorklund K, Li LY (2017) Adsorption of organic stormwater pollutants onto activated carbon from sewage sludge. *J Environ Manag* 197:490–497. <https://doi.org/10.1016/j.jenvman.2017.04.011>
- China Paper Association (2023) China Paper Industry 2022 Annual Report, vol 44. China Pulp & Paper Industry, p 21–30+6 [https://kns.cnki.net/kcms2/article/abstract?v=0kbf0AymBCYyQN8as5Nacen2GJkvOjEzbmOiQwQS\\_rS9UOd7EFxtXsCLXtc19QgatawR5pNgHsZbRxyMamVIS5Q3OMI9jSR8OWKCKNltdb52m9iMWh9BXLxh7PrBp1V1m5gCZjcSWz3c6uuKUFFA==&uniplatform=NZKPT&language=CHS](https://kns.cnki.net/kcms2/article/abstract?v=0kbf0AymBCYyQN8as5Nacen2GJkvOjEzbmOiQwQS_rS9UOd7EFxtXsCLXtc19QgatawR5pNgHsZbRxyMamVIS5Q3OMI9jSR8OWKCKNltdb52m9iMWh9BXLxh7PrBp1V1m5gCZjcSWz3c6uuKUFFA==&uniplatform=NZKPT&language=CHS)
- Priadi C, Wulandari D, Rahmatika I, Moersidik SS (2014) Biogas production in the anaerobic digestion of paper sludge. *APCBEE Proc* 9:65–69. <https://doi.org/10.1016/j.apcbec.2014.01.012>
- Mphahlele K, Matjie RH, Osifo PO (2021) Thermodynamics, kinetics and thermal decomposition characteristics of sewage sludge during slow pyrolysis. *J Environ Manag* 284. <https://doi.org/10.1016/j.jenvman.2021.112006>
- Cheng F, Luo H, Hu L, Yu B, Luo Z, Fidalgo de Cortalezzi M (2016) Sludge carbonization and activation: From hazardous waste to functional materials for water treatment. *J Environ Chem Eng* 4(4):4574–4586. <https://doi.org/10.1016/j.jece.2016.11.013>
- Zhu G, Zhu X, Xiao Z, Zhou R, Zhu Y, Wan X (2013) Kinetics of peanut shell pyrolysis and hydrolysis in subcritical water. *J Mater Cycles Waste Manage* 16(3):546–556. <https://doi.org/10.1007/s10163-013-0209-7>
- Park J, Lee Y, Ryu C, Park Y-K (2014) Slow pyrolysis of rice straw: analysis of products properties, carbon and energy yields. *Bioresour Technol* 155:63–70. <https://doi.org/10.1016/j.biortech.2013.12.084>
- Park HJ, Heo HS, Park Y-K, Yim J-H, Jeon J-K, Park J, Ryu C, Kim S-S (2010) Clean bio-oil production from fast pyrolysis of sewage sludge: effects of reaction conditions and metal oxide catalysts. *Bioresour Technol* 101:S83–S85. <https://doi.org/10.1016/j.biortech.2009.06.103>
- Gao N, Quan C, Liu B, Li Z, Wu C, Li A (2017) Continuous pyrolysis of sewage sludge in a screw-feeding reactor: products characterization and ecological risk assessment of heavy metals. *Energy Fuel* 31(5):5063–5072. <https://doi.org/10.1021/acs.energyfuels.6b03112>
- Wang C, Bi H, Lin Q, Jiang X, Jiang C (2020) Co-pyrolysis of sewage sludge and rice husk by TG–FTIR–MS: pyrolysis behavior, kinetics, and condensable/non-condensable gases characteristics. *Renew Energy* 160:1048–1066. <https://doi.org/10.1016/j.renene.2020.07.046>
- Fang S, Yu Z, Lin Y, Hu S, Liao Y, Ma X (2015) Thermogravimetric analysis of the co-pyrolysis of paper sludge and municipal solid waste. *Energy Convers Manag* 101:626–631. <https://doi.org/10.1016/j.enconman.2015.06.026>
- Zhao B, Xu X, Li H, Chen X, Zeng F (2018) Kinetics evaluation and thermal decomposition characteristics of co-pyrolysis of municipal sewage sludge and hazelnut shell. *Bioresour Technol* 247:21–29. <https://doi.org/10.1016/j.biortech.2017.09.008>
- Huang H, Liu J, Liu H, Evrendilek F, Buyukada M (2020) Pyrolysis of water hyacinth biomass parts: Bioenergy, gas emissions, and by-products using TG–FTIR and Py–GC/MS analyses. *Energy Convers Manag* 207. <https://doi.org/10.1016/j.enconman.2020.112552>
- Cai H, Zou H, Liu J, Xie W, Kuo J, Buyukada M, Evrendilek F (2018) Thermal degradations and processes of waste tea and tea leaves via TG–FTIR: combustion performances, kinetics, thermodynamics, products and optimization. *Bioresour Technol* 268:715–725. <https://doi.org/10.1016/j.biortech.2018.08.068>
- Wang Z, Xie L, Liu K, Wang J, Zhu H, Song Q, Shu X (2019) Co-pyrolysis of sewage sludge and cotton stalks. *Waste Manag* 89:430–438. <https://doi.org/10.1016/j.wasman.2019.04.033>
- Domínguez A, Fernández Y, Fidalgo B, Pis JJ, Menéndez JA (2008) Bio-syngas production with low concentrations of CO<sub>2</sub> and CH<sub>4</sub> from microwave-induced pyrolysis of wet and dried sewage sludge. *Chemosphere*. 70(3):397–403. <https://doi.org/10.1016/j.chemosphere.2007.06.075>
- Zhang Y, Wang J, Lv P, Bie N, Cao P, Bai Y, Song X, Yu G (2022) Capture of released alkali metals and its simultaneously catalytic performance on secondary reactions of volatiles during biomass pyrolysis. *Fuel*. 317. <https://doi.org/10.1016/j.fuel.2022.123557>
- Zhao Y, Yue J, Tao L, Liu Y, Shi SQ, Cai L, Xiao S (2020) Effect of lignin on the self-bonding of a natural fiber material in a hydro-thermal environment: lignin structure and characterization. *Int J Biol Macromol* 158:1135–1140. <https://doi.org/10.1016/j.ijbmac.2020.04.060>
- Xu Q, Tang S, Wang J, Ko JH (2018) Pyrolysis kinetics of sewage sludge and its biochar characteristics. *Process Saf Environ Prot* 115:49–56. <https://doi.org/10.1016/j.psep.2017.10.014>
- Alvarez J, Amutio M, Lopez G, Bilbao J, Olazar M (2015) Fast co-pyrolysis of sewage sludge and lignocellulosic biomass in a conical spouted bed reactor. *Fuel*. 159:810–818. <https://doi.org/10.1016/j.fuel.2015.07.039>
- Cai H, Liu J, Xie W, Kuo J, Buyukada M, Evrendilek F (2019) Pyrolytic kinetics, reaction mechanisms and products of waste tea via TG–FTIR and Py–GC/MS. *Energy Convers Manag* 184:436–447. <https://doi.org/10.1016/j.enconman.2019.01.031>
- Lin Y, Liao Y, Yu Z, Fang S, Lin Y, Fan Y, Peng X, Ma X (2016) Co-pyrolysis kinetics of sewage sludge and oil shale thermal decomposition using TGA–FTIR analysis. *Energy Convers Manag* 118:345–352. <https://doi.org/10.1016/j.enconman.2016.04.004>
- Han TU, Kim Y-M, Watanabe C, Teramae N, Park Y-K, Kim S, Lee Y (2015) Analytical pyrolysis properties of waste medium-density fiberboard and particle board. *J Ind Eng Chem* 32:345–352. <https://doi.org/10.1016/j.jiec.2015.09.008>
- Zhang J, Zhao R, Du Y, Chen L, Chen Z, Xiao N, Wu Z (2022) Study on the co-pyrolysis characteristics of sewage sludge and wood powder and kinetic analysis. *Biomass Convers Biorefinery*. <https://doi.org/10.1007/s13399-022-02589-9>
- Tao W, Duan W, Liu C, Zhu D, Si X, Zhu R, Oleszczuk P, Pan B (2020) Formation of persistent free radicals in biochar derived

- from rice straw based on a detailed analysis of pyrolysis kinetics. *Sci Total Environ* 715. <https://doi.org/10.1016/j.scitotenv.2020.136575>
26. Shahbeig H, Nosrati M (2020) Pyrolysis of municipal sewage sludge for bioenergy production: thermo-kinetic studies, evolved gas analysis, and techno-socio-economic assessment. *Renew Sust Energ Rev* 119. <https://doi.org/10.1016/j.rser.2019.109567>
  27. Wang B, Xu F, Zong P, Zhang J, Tian Y, Qiao Y (2019) Effects of heating rate on fast pyrolysis behavior and product distribution of Jerusalem artichoke stalk by using TG-FTIR and Py-GC/MS. *Renew Energy* 132:486–496. <https://doi.org/10.1016/j.renene.2018.08.021>
  28. Tsemame MM, Matjie RH, Bunt JR, Neomagus HWJP, Strydom CA, Waanders FB, Van Alphen C, Uwaoma R (2019) Mineralogy and petrology of chars produced by South African caking coals and density-separated fractions during pyrolysis and their effects on caking propensity. *Energy Fuel* 33(8):7645–7658. <https://doi.org/10.1021/acs.energyfuels.9b01275>
  29. Zaker A, Chen Z, Zaheer-Uddin M, Guo J (2021) Co-pyrolysis of sewage sludge and low-density polyethylene – a thermogravimetric study of thermo-kinetics and thermodynamic parameters. *J Environ Chem Eng* 9(1). <https://doi.org/10.1016/j.jece.2020.104554>
  30. Liu Y, Song Y, Fu J, Ao W, Ali Siyal A, Zhou C, Liu C, Yu M, Zhang Y, Dai J, Bi X (2022) Co-pyrolysis of sewage sludge and lignocellulosic biomass: synergistic effects on products characteristics and kinetics. *Energy Convers Manag* 268. <https://doi.org/10.1016/j.enconman.2022.116061>
  31. Marforio TD, Bottoni A, Zerbetto F, Calvaresi M (2019) CNT-catalyzed oxidative dehydrogenation of ethylbenzene to styrene: DFT calculations disclose the pathways. *ChemNanoMat*. 5(4):499–505. <https://doi.org/10.1002/cnma.201800558>
  32. Wang C, Wang T, Hu Z, Cai Z (2020) Facile synthesis and thermal performance of cetyl palmitate/nickel foam composite phase change materials for thermal energy storage. *J Energy Storage* 28. <https://doi.org/10.1016/j.est.2019.101179>
  33. Liu H, Li D, Li R, Sun H, Zhang Y, Zhang L, Zhao P (2017) Synthesis of pentaerythritol stearate ester-based zinc alkoxide and its synergistic effect with calcium stearate and zinc stearate on PVC thermal stability. *J Vinyl Addit Technol* 24(4):314–323. <https://doi.org/10.1002/vnl.21602>
  34. Venkataraman S, Athilakshmi JK, Rajendran DS, Bharathi P, Kumar VV (2024) A comprehensive review of eclectic approaches to the biological synthesis of vanillin and their application towards the food sector. *Food Sci Biotechnol*. <https://doi.org/10.1007/s10068-023-01484-x>
  35. Takikawa G, Katagiri T, Uneyama K (2005) Preparation and synthetic application of a novel ketene silyl acetal of methyl trifluoropyruvate. *J Organomet Chem* 70:8811–8816. <https://doi.org/10.1021/jo051242q>
- Publisher's Note** Springer Nature remains neutral with regard to jurisdictional claims in published maps and institutional affiliations.
- Springer Nature or its licensor (e.g. a society or other partner) holds exclusive rights to this article under a publishing agreement with the author(s) or other rightsholder(s); author self-archiving of the accepted manuscript version of this article is solely governed by the terms of such publishing agreement and applicable law.